Applied Catalysis B: Environmental 189 (2016) 75–85

Contents lists available at ScienceDirect

Applied Catalysis B: Environmental

journal homepage: www.elsevier.com/locate/apcatb

Nanostructured $BaTiO_3/Cu_2O$ heterojunction with improved photoelectrochemical activity for H_2 evolution: Experimental and first-principles analysis

Dipika Sharma[a], Sumant Upadhyay[a], Vibha R. Satsangi[b], Rohit Shrivastav[a], Umesh V. Waghmare[c], Sahab Dass[a,*]

[a] Department of Chemistry, Dayalbagh Educational Institute, Agra 282 110, India
[b] Department of Physics & Computer Sciences, Dayalbagh Educational Institute, Agra 282 110, India
[c] Theoretical Sciences Unit, Jawaharlal Nehru Centre for Advanced Scientific Research, Jakkur, Bangalore 560 064, India

ARTICLE INFO

Article history:
Received 29 December 2014
Received in revised form
15 September 2015
Accepted 16 February 2016
Available online 21 February 2016

Keyword:
Heterojunction
Spray pyrolysis
Sol-gel
Photoelectrochemical
Effective mass
band offset

ABSTRACT

Nanostructured $BaTiO_3/Cu_2O$ heterojunction electrodes with varying thickness of Cu_2O thin films were synthesized using spray deposition of porous cuprous oxide films onto the surface of spin coated nanostructured thin films of $BaTiO_3$. First-principles based density functional theory calculations have been done for the first time on the band offsets of $BaTiO_3/Cu_2O$ heterojunction interface and effective mass of electron and hole for bulk $BaTiO_3$ and Cu_2O, exhibited better separation of the photogenerated charge carriers at the $BaTiO_3/Cu_2O$ interface. Experimental results on photoelectrochemical activity of $BaTiO_3/Cu_2O$ heterojunction in the photoelectrochemical cell for water splitting reaction validate the theoretical results. Maximum photocurrent density value of 1.44 mA/cm^2 at 0.95 V/SCE was observed for $BaTiO_3/Cu_2O$ heterojunction photoelectrode with 442 nm thickness. Photo-generated charge carriers apparently transfer more easily in $BaTiO_3/Cu_2O$ heterojunction than that in pristine Cu_2O and $BaTiO_3$.

1. Introduction

Various Strategies have been attempted to improve performance of photoelectrodes in the Photoelectrochemical splitting of water including dye sensitization [1] or using inorganic sensitizers [2], doping [3,4], swift heavy ion irradiation [5], use of heterojunction or layered systems [6,7]. Overall performance of PEC water splitting process is limited by efficiency of photogenerated charge carriers separation and their rate of electron transfer to the reaction site [8–10]. An efficient charge separation at the interface is still a challenge before the researchers and scientific community at large. Bilayered/heterojunction system of metal oxide semiconductors is one of the recent strategies towards improving the performance of the photocatalyst with inherent merits [11–20]. Use of *p-n* heterojunction as a building block for nanodevices [21–25] is preferred over single semiconductors [26], because *p-n* junction creates a region with potential gradient near which electrons in n-type semiconductors and holes in p-type semiconductors are depleted, and potential gradient thus generated facilitates the separation of charge carriers thereby reducing the recombination of electrons and holes. $BaTiO_3$ can be consider as a good photoelectrode for photoelectrochemical water splitting as it has high resistance to corrosion and photocorrosion in aqueous media and well-matched energy band edges with the redox level of water, However, $BaTiO_3$ band gap is about 3.2 eV and it mostly absorbs in the ultraviolet region of spectrum with a small amount of visible light [27] Combination of n-type $BaTiO_3$ with p-type semiconductor such as Cu_2O, MoS_2, CuO to form *p-n* heterojunction can be a effective way to improve the absorption in visible light and separation of photogenerated charge carriers. Among these p-type semiconductors Cu_2O is highlighted due to its low band gap (Eg = 2.2 eV) and promising material for conversion of solar energy into electrical or chemical energy [28]. Moreover, one of the physical quantities that play an important role in characterizing the interface of semiconductor heterojunction systems is the band offset, i.e., relative position of the energy levels on both sides of the interface. Difference between the positions of the top of the valence bands and bottom of the conduction bands of the two materials is valence band offset (VBO) and conduction band offset (CBO) respectively. These band discontinu-

* Corresponding author.
E-mail addresses: vibhasatsangi@gmail.com (V.R. Satsangi), waghmare@jncasr.ac.in (U.V. Waghmare), drsahabdas@gmail.com (S. Dass).

http://dx.doi.org/10.1016/j.apcatb.2016.02.037
0926-3373/

ities play a fundamental role in deciding the transport properties of heterojunction systems. With this idea, this paper presents the First-principles density functional pseudopotential calculations on the band offsets of $BaTiO_3/Cu_2O$ heterojunction interface and effective mass of electron and hole for bulk $BaTiO_3$ and Cu_2O to explain the better separation of the photogenerated charge carriers at the $BaTiO_3/Cu_2O$ interface and their experimental validations on photoelectrochemical response of nanostructured $BaTiO_3$ thin films modified by overlayering of Cu_2O with varying thickness. Prepared $BaTiO_3/Cu_2O$ heterojunction photoelectrodes were also characterized for their structural, electrical and optical properties to assess the mechanism by which this concept influences the photoelectrode performance.

2. Experimental

Copper(II) acetate [$Cu(CH_3COO)_2{\cdot}H_2O$, Aldrich 98%], Dextrose [Fisher 99.5%] and isopropanol [$(CH_3)_2CHOH$, Qualigens 99.5%] were used for cuprous oxide synthesis. For the synthesis of $BaTiO_3$, barium acetate [$Ba(CH_3COO)_2$, Aldrich 99%], titanium(IV) isopropoxide [$Ti(OC_2H_4CH_3)_4$, Aldrich 99%], 2-methoxyethanol [$CH_3OCH_2CH_2OH$, Aldrich 99.3%] and glacial acetic acid [CH_3COOH, Qualigens, 99.5%], were used as precursor solution.

2.1. Preparation of photoelectrode

2.1.1. Preparation of nanostructured $BaTiO_3$ thin films

Nanostructured thin films of $BaTiO_3$ were deposited on ITO (Sn: In_2O_3) glass substrate using sol-gel spin coating method. The precursor solution comprising of barium acetate [$Ba(CH_3COO)_2$] and titanium isopropoxide [$Ti(OC_2H_4CH_3)_4$] dissolved in glacial acetic acid (CH_3COOH) and 2-methoxyethanol ($CH_3OCH_2CH_2OH$). Initially an appropriate ratio of solid-state barium acetate was dissolved in glacial acetic acid. In second step stoichiometric amount of titanium isopropoxide was dissolved in 2-methoxyethanol with stirring at 70 °C for 30 mins and cooled to room temperature. Both solutions were then mixed with each other for making stoichiometric, transparent, and stable Barium titanate precursor. The films were spin coated on ITO at 2000 rpm for 20 s and sintered at 600 °C for 2 h [29]. Finally films were slowly cooled to room temperature inside the furnace. One third length of ITO substrate was initially covered by transparent tape to establish the electrical contact to convert them into electrodes. Synthesis of $BaTiO_3$ thin films from acetate precursor shown in the following flow chart:

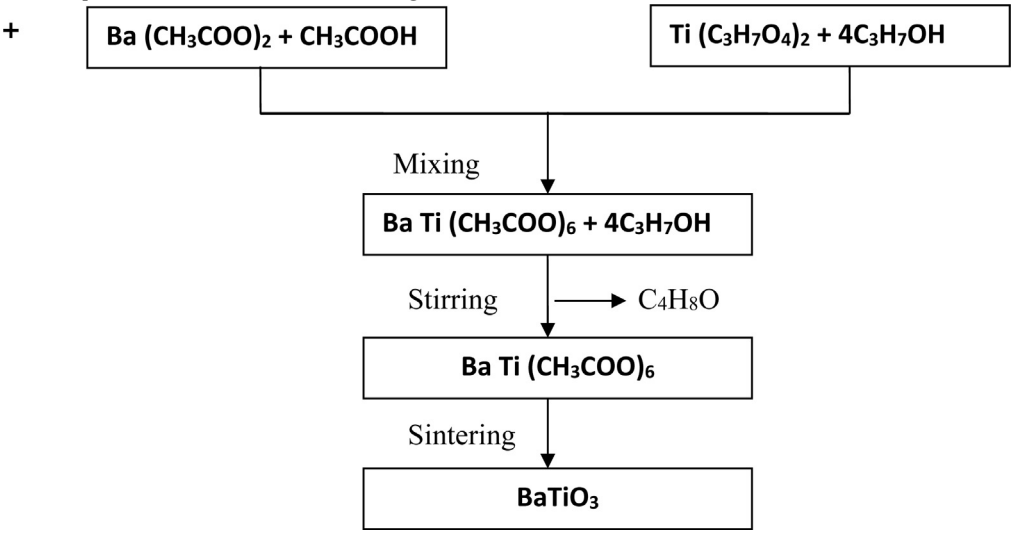

Table 1
Thicknesses with other details of samples.

Film thickness (nm)				
S.no.	Cu_2O	$BaTiO_3$	overall thickness	Acronym
1	142	–	142	A
2	–	156	156	B
3	142	156	298	C
4	286	156	442	D
5	307	156	463	E
6	541	156	697	F

2.1.2. Preparation of $BaTiO_3/Cu_2O$ heterojunction thin films

Nanostructured $BaTiO_3/Cu_2O$ heterojunction thin films were obtained by deposition of Cu_2O thin film layer with varying thickness over the predeposited $BaTiO_3$ thin film by spray pyrolysis method (Holmarc, India). The precursor solution containing of Copper(II) acetate monohydrate ($Cu(CH_3COO)_2{\cdot}H_2O$), and Dextrose dissolved in water were used as starting compounds. In addition 20 vol% of 2-propanol [$(CH_3)_2CHOH$ (Qualigens 99.5%)] was added to the above described aqueous solution. Detailed methodology has been reported elsewhere [30]. To optimize the photoelectrochemical response of $BaTiO_3/Cu_2O$ heterojunction thin films, 15, 30, 45 and 60 s spray periods were tried for the deposition of Cu_2O thin films. The possible chemical reactions for the formation of Cu_2O crystal are shows given below:

$$Cu(CH_3COO)_2.H_2O \xrightarrow{aq} 2Cu^{2+} + CH_2COO^- + H_2O$$

$$2Cu^{2+} + C_6H_{12}O_6 + H_2O \rightarrow 2Cu^{+} + C_6H_{12}O_7 + 2H^{+}$$

$$2Cu^{+} + 2H_2O + OH^{-} \rightarrow Cu_2O + 4H^{+} + H_2O$$

Thicknesses with other details of samples prepared have been summarized in Table 1. To use $BaTiO_3/Cu_2O$ heterojunction thin films as photoelectrode in PEC cell, electrical contacts were obtained using silver paste and copper wire, from the uncoated area of the conducting glass substrate. The area of contact was later covered with non-transparent and non-conducting epoxy-resin (Hysol, Singapore). The effective area of the photoelectrode available for illumination was 1.0 cm^2.

3. Characterization

Cross-sectional and surface morphology of samples was characterized using field emission scanning electron microscope

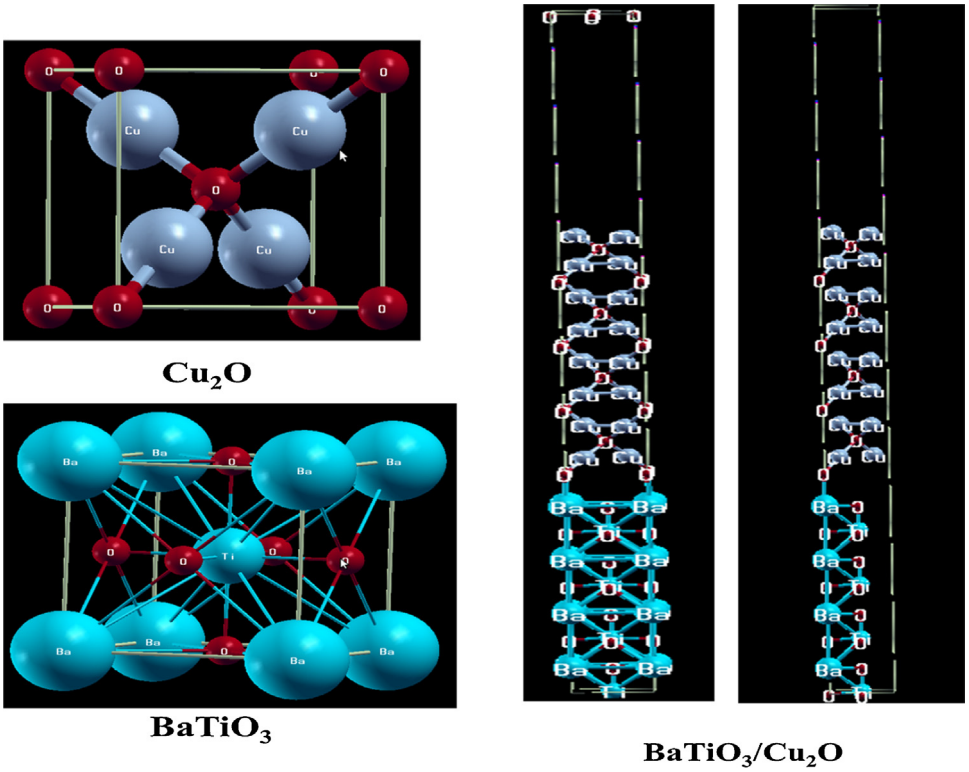

Fig 1. Supercell model considered in the present work.

(FE-SEM), (INCA Penta FET X3, TESCAN, Inter University Accelerator Centre, New Delhi) and (Hitachi S3700, Japan) respectively. X-ray diffraction (XRD) patterns, obtained to characterized the crystalline phase structure and size of the particles on Bruker AXS, Germany X-ray diffractogram (model D8 Advance), having Cu Ka (λ = 1.5418A°) radiation in the scanning angle range (20–60°) 2θ. UV–vis absorption spectra were recorded on a UV–vis spectrophotometer (Shimadzu, Japan, Model: UV-2450). The thickness of samples was measured using alpha-step profilometer (tencor Alpha Step D-120). Photoelectrochemical measurements were performed in a three electrode system PEC cell. Pt gauze and saturated calomel (PAR, Model: K0077, USA) was used as counter electrode and reference electrode respectively, and all prepared samples with an exposure area of 1 cm^2 were used as working electrode. All electrodes were dipped in aqueous electrolyte of 0.1MNaOH. A 150 W xenon arc lamp equipped with a water filter was used to remove the IR energy and to avoid overheating was utilized as the UV–vis light source. The integrated light intensity was 150 m W cm^{-2}. Current–voltage curves were recorded using scanning potentiostat (PAR, Model: VersaStat II, USA), under darkness and by illuminating the photoelectrode at a scan rate of 20 mV/s. The slope of Current–voltage curves under darkness was employed to calculate the resistivity for all the samples. The open circuit potential (V_{oc}) was also measured in order to calculate applied bias photon-to-current efficiency under illumination for all the samples. The incident photon to electron conversion efficiency (IPCE) of the samples was measured using electrochemical workstation (Zahner, PP211, CIMPS-pcs, Germany) with wideband white LED tuneable light source (output intensity = 1.02 W/m^{-2}) and calculated as follows:

$$\mathrm{IPCE} = \frac{1240\mathrm{I}}{\lambda \mathrm{J}_{\mathrm{Light}}}$$

where J is the measured photocurrent density, λ is the wavelength of the incident light, and I light is the measured irradiance at the measurement wavelength [31].

3.1. Details of the density functional theory simulations

The calculations have been performed using the Quantum Espresso package [32] within the framework of density functional theory by adopting the generalized gradient approximation (GGA) of PBE functional [33] for the exchange correlation potential. Ultrasoft pseudopotentials [34] were used in the description of the electron–ion interactions. A Monkhorst-pack mesh [35] of 8 2 points was used in sampling the integrals over the brillouin zone, and a much finer mesh was used for accurate determination of the density of the electronic states. The electron wave function was expanded in a plane wave basis set with an energy cutoff 30 Ry, and the charge density was represented with a plane-wave basis with a cutoff of 180 Ry. Structural optimization was carried out using Hellman-Feynman forces to minimize the total energy. Electronic structures reported have been calculated at the optimized structures.

3.2. Model of the $BaTiO_3/Cu_2O$ interface

The band alignment at semiconductor interfaces can be theoretically computed by the construction of supercell using periodic slab models. Supercell must be periodic in three dimensions and large enough to describe both bulk and interface properties of Cu_2O and $BaTiO_3$. In this study $BaTiO_3/Cu_2O$ interface is modelled, within the supercell method, by a slab consisting of four unit cell of Cu_2O (0 0 1) on the top of four $BaTiO_3$ (0 0 1) unit cell (see Fig. 1). This atomic arrangement leads to a polar crystal along the longitudinal c-axis. We also use a thick layer of vacuum to minimize the effects of polarity and periodic images associated with the supercell.

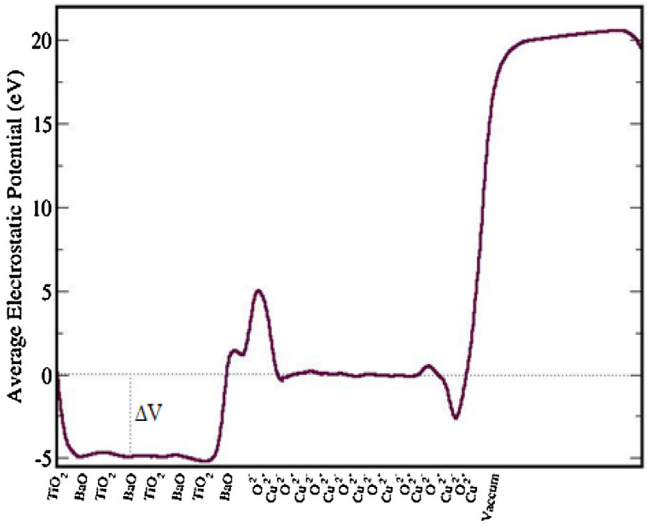

Fig. 2. Macroscopically average electrostatic potential where the averaging steps along the Z-direction of the $BaTiO_3/Cu_2O$ supercell.

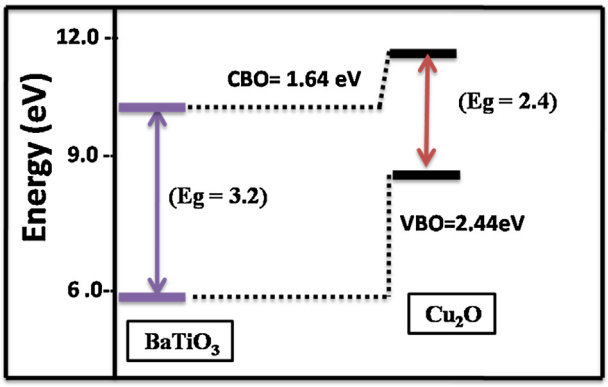

Fig. 3. Schematic representation of band structures discontinuities at $BaTiO_3/Cu_2O$ heterojunction.

4. Result and discussion

4.1. Theoretical results

4.1.1. Band offsets calculations

The transport properties in semiconductor heterojunction systems are controlled by the electronic band profiles at the interfaces, more specifically by the valence and conduction discontinuities that accommodate the difference in band gap between the materials, the valence and conduction band offsets (VBO and CBO). These discontinuities determination using first-principles cannot be achieved by the bulk properties of the constituents. So it is prudent to consider the lineup of microscopic average potential between the two materials. This potential shift depends on the dipole induced by the electronic charge transferred from one part of the interface to the other after the interfacial hybridization. Theoretical investigations of the band offsets (BO) are usually split into two terms [36,37]:

$$BO = \Delta Ev, c + \Delta V \quad (1)$$

The first contribution (ΔEv and ΔEc), is referred to as the band-structure term. Knowing the value of ΔEv, we can simply obtain ΔEc by adding the experimental band gaps. The second term, ΔV, is the step-like jump in the average of the electrostatic potential across the heterojunction, and is obtained using planar and macroscopic averages of the electrostatic potential (see Fig. 2). Obtained values of valence band and conduction band offsets for $BaTiO_3/Cu_2O$ heterojunction using are given in Table 2.

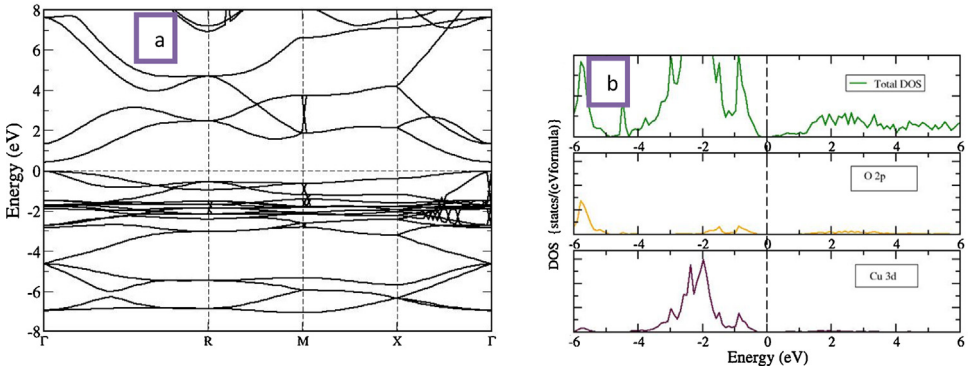

Fig. 4. (a, b) Band structure and DOS for bulk Cu_2O.

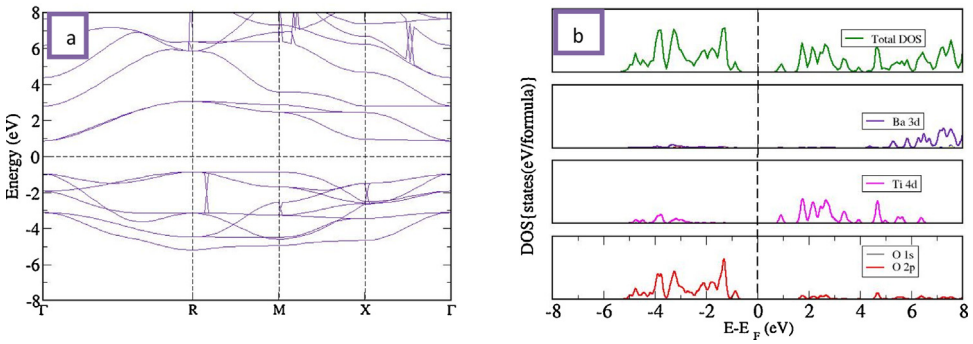

Fig. 5. (a, b) Band structure and DOS for bulk $BaTiO_3$.

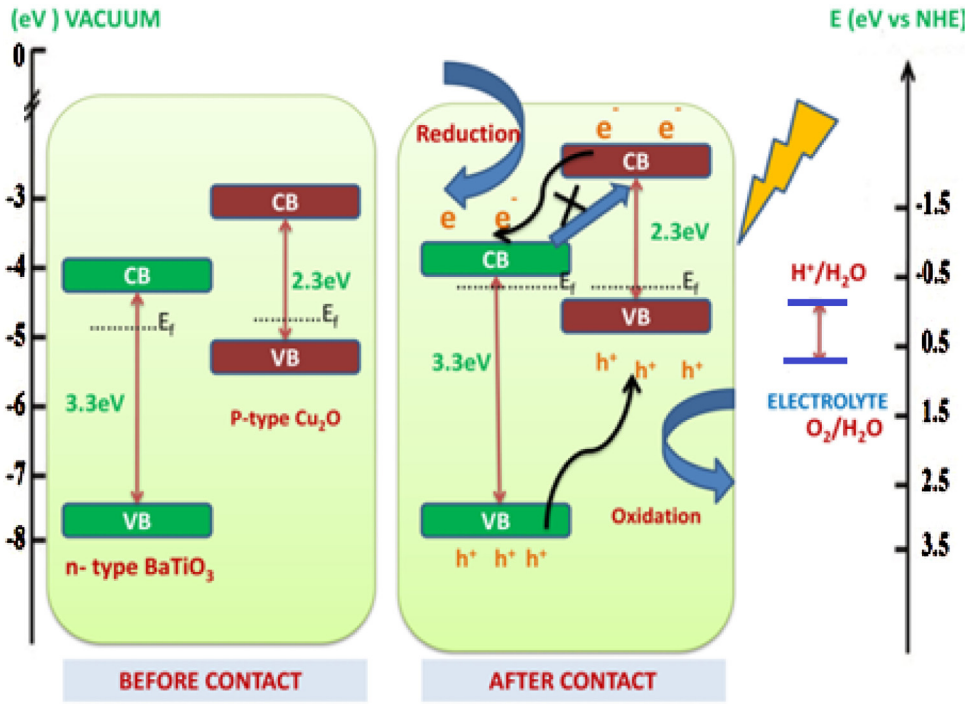

Fig. 6. Energy Band diagram of Cu_2O and $BaTiO_3$ before and after formation of *p-n* junction.

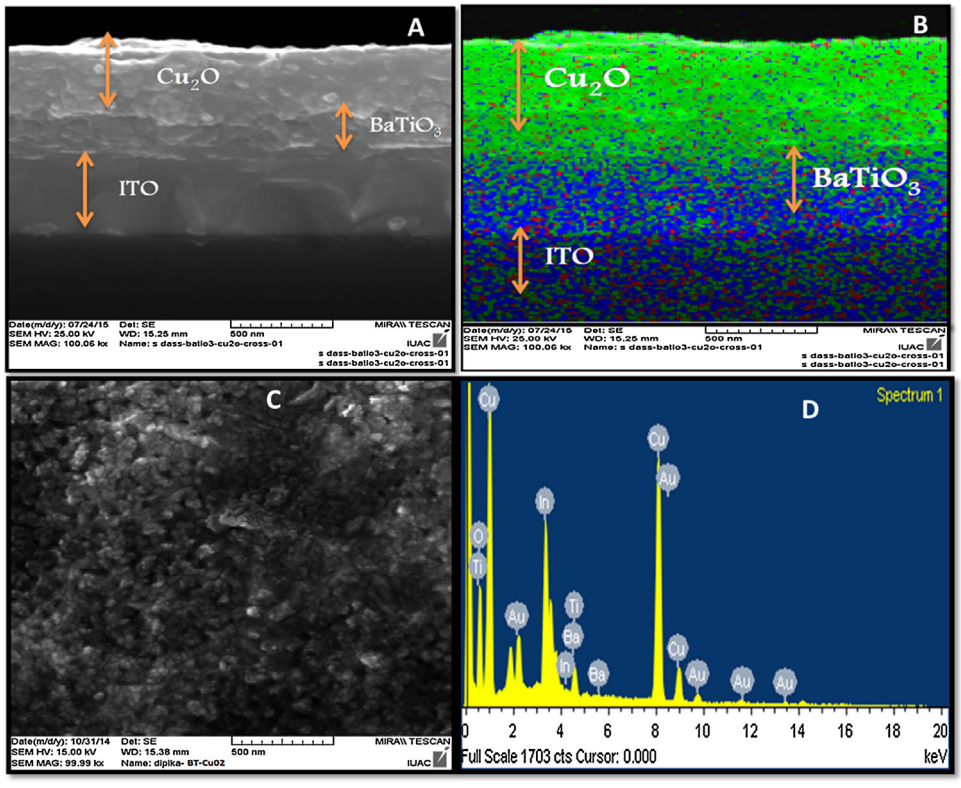

Fig. 7. (A) Cross-sectional SEM image, (B) Coloured cross-sectional SEM image (C) SEM image (D) Energy dispersive X-ray image of $BaTiO_3/Cu_2O$ heterojunction sample 'D'.

Table 2
Valence band and Conduction band offsets for $BaTiO_3/Cu_2O$ system.

ΔEv	ΔEc	ΔV	VBO	CBO
2.7 eV	3.5 eV	−5.14 eV	2.44 eV	1.64 eV

Fig. 3 shows a schematic representation of the band structure discontinuities for the $BaTiO_3/Cu_2O$ heterojunction interface such as VBO and CBO calculated as given in Eq. (1). A positive value of the band offset for the discontinuity at $BaTiO_3/Cu_2O$ heterojunction indicates an upward shift from $BaTiO_3$ to Cu_2O [38].

Table 3
Effective mass components (in unit of m_0).

	Cu_2O	$BaTiO_3$
CBM at Γ point Γ-R (111) Direction	0.676	0.918
VBM at Γ point Γ-R (111) Direction	3.80	1.67
VBM at M point M-X (110) Direction	–	1.348

From these results we conclude that $BaTiO_3/Cu_2O$ heterojunction interface is type-II or having staggered type band edges alignment after contact, which favours the charge carrier separation or photoelectrochemical activity. Furthermore, conductivity of material depends on the mobility of electron and holes while, mobility is proportional to the reciprocal of effective mass which is the intrinsic property of the material. To find out the mobility and their movement across the heterojunction interface effective mass of electron and holes is also calculated for $BaTiO_3$ and Cu_2O at conduction band minima and valence band maxima.

4.1.2. Effective mass calculation

The effective mass of electron m_e at the conduction band minima and hole m_h at valence band maxima for $BaTiO_3$ and Cu_2O were evaluated by fitting the conduction and valence bands to a parabola according to $E = \frac{h^2k^2}{2m_e m_0}$, where m_0 denotes the electron rest mass [39]. Conduction band minima and valence band maxima of Cu_2O lie at same point (Γ) indicating its direct band gap behaviour shown in Fig. 4(a) [40]. In contrast to it in case of $BaTiO_3$ it can be seen that the conduction band minima and valence band maxima lie at different points indicating it to be a indirect band gap semiconductor Fig. 5(a) [41]. DOS calculations show that conduction band and valence band of Cu_2O is mainly constructed by O-2p orbitals and Cu-3d orbitals and $BaTiO_3$ constructed with Ba-3d, Ti-4d and O-2p orbitals respectively [Figs. 4(b) 5(b)]. Electron effective mass for Cu_2O and $BaTiO_3$ calculated at CBM near Γ point in Γ-R direction and hole effective mass at VBM in different directions shown in Table 3 [42,43]. From the calculated values of effective masses,

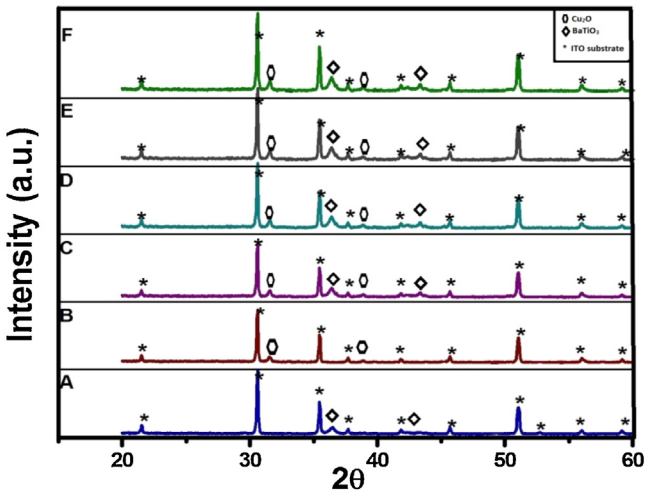

Fig. 8. X-ray diffraction pattern for pristine Cu_2O (A), $BaTiO_3$ (B) and heterojunction $BaTiO_3/Cu_2O$ (C,D,E,F) thin films Asterisks indicate the peaks corresponding to underlying ITO conducting glass substrate.

it is clear that elctrons in Cu_2O have high mobilty as compared to electron present in $BaTiO_3$. Contray to this hole mobility is higher in $BaTiO_3$. Theoretical results clearly demonstrate that $BaTiO_3/Cu_2O$ junction having type II (staggered type) band edges alignment and favourable mobility of charge carriers for better charge separation at the interface [44].

4.2. Experimental results

Heterojunction of Cu_2O and $BaTiO_3$ having staggered band-edge alignment (i.e., type-II band alignment) i.e., valence band (VB) of Cu_2O being more positive than the Valence band (VB) of $BaTiO_3$ and conduction band (CB) of Cu_2O is more negative that of CB of $BaTiO_3$ to improve the charge carrier separation as shown in

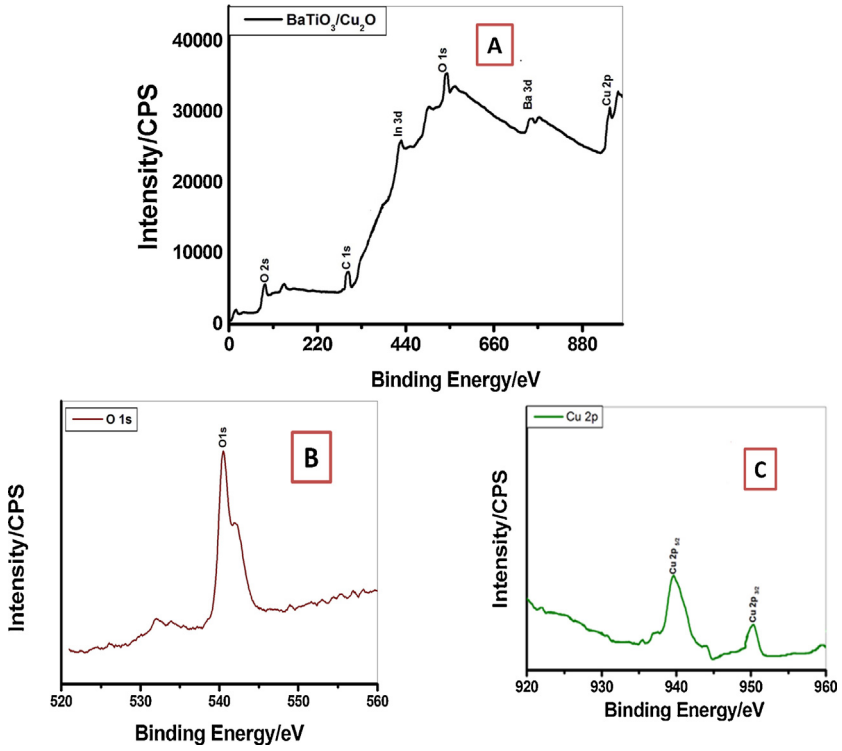

Fig. 9. XPS spectra of (A) full-spectrum scan, (B) High resolution spectrum of O 1s (C) Cu 2p for $BaTiO_3/Cu_2O$ heterojunction (sample D).

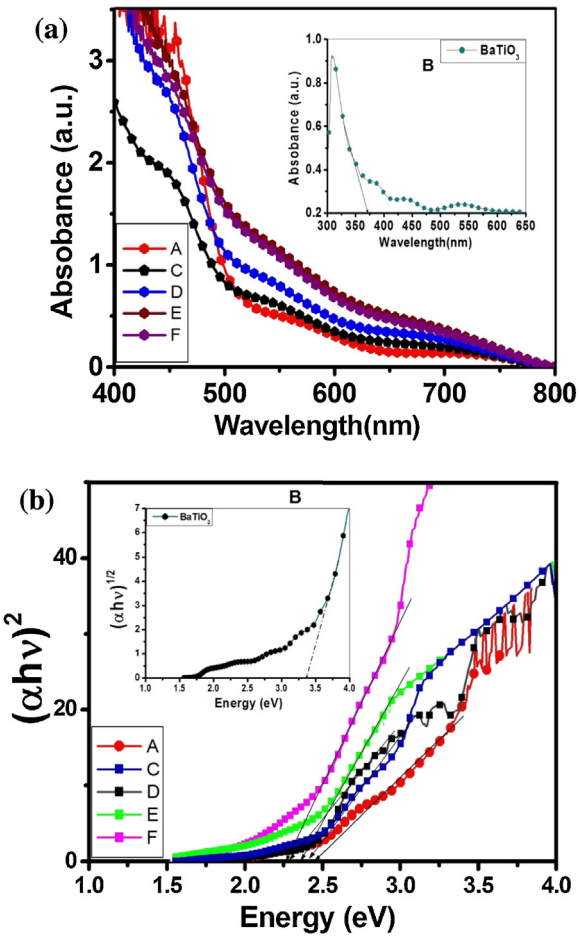

Fig. 10. (a) UV–vis absorption spectra for pristine Cu_2O(A), $BaTiO_3$ (B), and heterojunction $BaTiO_3/Cu_2O$ (C,D,E,F) thin film samples with overall thickness of 294 nm, 442 nm, 463 nm and 697 nm respectively. (b) Tauc plots for pristine Cu_2O (A), $BaTiO_3$ (B), and heterojunction $BaTiO_3/Cu_2O$ (C, D, E, F) thin film samples with overall thickness of 294 nm, 442 nm, 463 nm and 697 nm respectively.

Fig. 6. We attempted to validate the theoretical results by sensitizing $BaTiO_3$ with Cu_2O. $BaTiO_3/Cu_2O$ heterojunction could be beneficial because of the separation of charge carriers and better absorption of light in PEC water splitting.

4.2.1. SEM analysis

Fig. 7(A-B), (D) depict a typical Cross-sectional SEM, coloured Cross-sectional SEM and Energy dispersive X-ray image of $BaTiO_3/Cu_2O$ heterojunction sample (with overall thickness of 442 nm i.e., sample D). Cross SEM image clearly shows the successful deposition of Cu_2O with more porosity on to uniform dense thin films of $BaTiO_3$ which is also clear in SEM image shown in [Fig. 7(c)] Thickness for $BaTiO_3$ and Cu_2O thin films calculated with cross SEM analysis were 160 nm and 278 nm respectively which are in good agreement with the values obtained from surface profilometer. EDAX image of same $BaTiO_3/Cu_2O$ heterojunction sample exhibits atomic percentage of the Ba, Ti, Cu and O was 3.33, 1.78, 56.18 and 36.43% respectively. SEM image for heterojunction sample (D) shown in Fig. 7(C) clearly indicate the porous morphology of Cu_2O with particle size of 25–25 nm while $BaTiO_3$ has dense and uniform deposition of particles with the size in the range of 40–45 nm. Porous morphology of Cu_2O may reduce the recombination of charge carriers in $BaTiO_3/Cu_2O$ heterojunction [45]

Table 4
Experimental lattice parameters obtained for $BaTiO_3$ and Cu_2O.

Material	Space group	Lattice Constant	Bond angle
Cu_2O	$P_n\bar{3}_m$	4.26	90°, 90°, 90°
$BaTiO_3$	P_m3_m	4.06	90°, 90°, 90°

4.2.2. XRD analysis

Fig. 8 shows the XRD pattern for pristine Cu_2O, $BaTiO_3$ and $BaTiO_3/Cu_2O$ heterojunctions. XRD is used to identify the crystal structure of the samples. Heterojunction thin films exhibited diffraction peaks at $2\theta = 36.53$, 42.43 which can be indexed to (1 1 1), (2 0 0) plane, respectively of the cubic cuprous oxide phase (JCPDS file no. 065–3288). Lattice constant of Cu_2O obtained is a = 4.26 Å, which is in agreement to the value a = 4.26 Å, of Cu_2O obtained by Yanchao Mao et al., 2012 [47]. The peaks at $2\theta = 31.5$, and 38.9°, can be indexed to (1 1 0) and (1 1 1) plane, respectively of the cubic barium titanate phase (JCPDS file no. 079–2263). The lattice constant of $BaTiO_3$ obtained from the present data is a = 4.06 Å [47]. Other experimental lattice parameters obtained for $BaTiO_3$ and Cu_2O from XRD analysis are shown in Table 4.The absence of any unidentified peak in case of heterojunction sample indicates that no mixed oxide has been formed. Comparing the XRD pattern of the pristine Cu_2O with that of the $BaTiO_3/Cu_2O$ samples reveals that peak corresponding to Cu_2O is markedly strengthened with increase in the thickness of Cu_2O. The crystallite size for Cu_2O thin film was calculated to be 27 nm from FWHM of most intense (1 1 1) diffraction peak using Debye-Scherrer's equation [48].

4.2.3. XPS analysis

Fig. 9 shows the XPS analysis on the $BaTiO_3/Cu_2O$ heterojunction sample D. The XPS survey scan spectra showed the presence of Ba, O, and Cu in the film. In the survey scan a low intensity peak for Ba is obtained as compared to Cu and O which may be due to presence of Cu_2O on the outer surface of the $BaTiO_3/Cu_2O$ heterojunction. The peak for C 1s at 284.8 eV is ascribed to adventitious carbon from the XPS instrument and peak at 538.7 eV is for O 1s region shown in Fig. 9B. In Fig. 9C XPS spectrum for Cu 2p shows two peaks at 932.5 eV and 952.7 eV that are assigned to Cu $2p_{3/2}$ and $2p_{1/2}$ respectively, which is a characteristic of Cu^+ in Cu_2O. As XPS is surface sensitive technique only Cu and O are appears in high resolution XPS for $BaTiO_3/Cu_2O$ heterojunction thin film [49,50]. XPS spectrum is also indicating the formation of heterojunction as revealed in XRD results.

4.2.4. Optical properties

The optical properties of the samples are studied by UV–Vis spectrometer as shown in Fig. 10(a). In contrast to pristine $BaTiO_3$ that has an absorption edge at approximately 375 nm with broad peaks at 400–450 nm and 500–600 nm which may be due to deep trap states F^+ centres associated with oxygen vacancies [51], absorbs in UV range while $BaTiO_3/Cu_2O$ heterojunction exhibits an increase in light absorption intensity and red-shift of absorption edge from 375 nm to 570 nm with increase in the thickness of Cu_2O thin film, indicating the narrowing of the band gap. A broad absorption from 500 to 600 nm which can be assigned to the $BaTiO_3/Cu_2O$ heterojunction, suggesting that photons can be simultaneously absorbed by both $BaTiO_3$ and Cu_2O which remarkably enhancing the light absorption ability. Interestingly, the absorption feature of the heterojunction is consistent more with Cu_2O thin film shown in Tauc plots Fig. 10(b), which may be due to synergic effect of Cu_2O thin films [52].

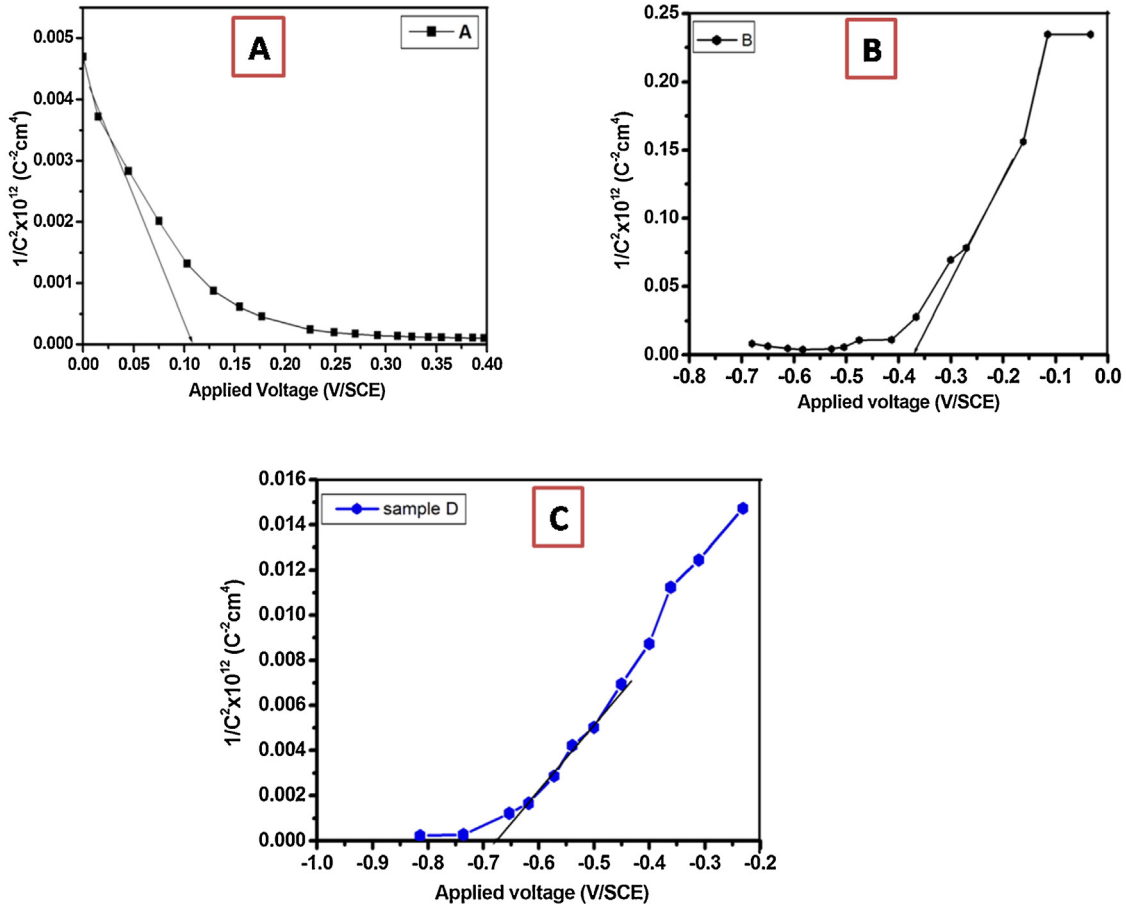

Fig. 11. Mott-Schottky curve for pristine Cu_2O (A), $BaTiO_3$ (B) and $BaTiO_3/Cu_2O$ sample (D).

4.2.5. Mott-Schottky analysis

The flatband potential (V_{fb}) is an important factor in deciding the performance of material at metal oxide/electrolyte junction and was estimated for pristine Cu_2O, $BaTiO_3$ and $BaTiO_3/Cu_2O$ sample(D) using Mott–Schottky curves (Fig. 11) by employing LCR meter (Agilent Technology, Model 4263B) based on equation

$$\frac{1}{C^2} = \left(\frac{2}{q\varepsilon_0\varepsilon_s N}\right)\left(V_{app} - V_{fb} - \frac{KT}{q}\right)$$

linear variations of $1/C^2$ with applied potential (V_{app}) were plotted to get Mott-Schottky (MS) curves. Here, q is the elementary charge, ε_0 and ε_s are permittivity of the vacuum and dielectric constant of semiconductor electrode respectively, V_{app} is the applied potential, k is the Boltzmann's constant, T is the absolute temperature and (kT/q) is a temperature dependent correction term. The capacitance at junction was measured, with varying potential, at 1 kHz signal frequency. The flat band potentials can be obtained from the linear fit of the data. Cu_2O show a negative slope in the linear region of the plot, indicating p-type characteristic. On the other side $BaTiO_3$ and $BaTiO_3/Cu_2O$ sample (D) film displays a positive slope, indicating the n-type behaviour. Although the Mott-Schottky plots obtained here were not as linear as expected in a bulk semiconductor electrode, which can be ascribed to varying stoichiometry from the two components in the film with different electronic properties [53]. Flatband potentials for pristine Cu_2O, $BaTiO_3$ and $BaTiO_3/Cu_2O$ sample (D) were 0.1, −0.375 and −0.71 V/SCE respectively. Maximum value of V_{fb} for $BaTiO_3/Cu_2O$ sample (D) with negative shift, also offered best photoelectrochemical response in this study indicating more charge separation of the charge carrier [54].

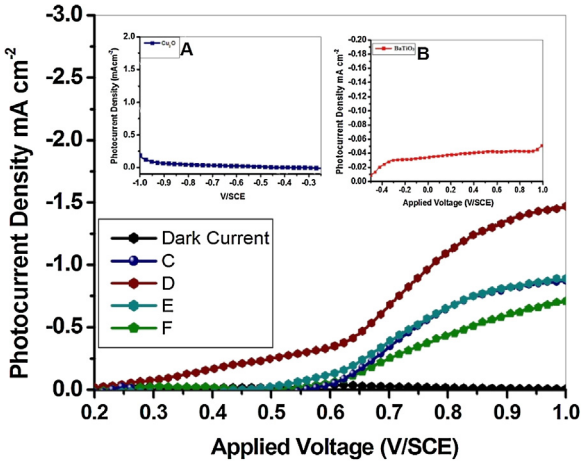

Fig. 12. Photocurrent density vs. Applied potential curve for Pristine Cu_2O (A), $BaTiO_3$ (B), and $BaTiO_3/Cu_2O$ heterojunction samples under UV–vis light illumination in 0.1 M NaOH electrolytic solution.

4.2.6. J-V curves

To examine the photoelectrochemical activity of the samples, linear sweep voltagrams were recorded both in the dark and under UV–vis light illumination to show the J–V plots. A higher photocurrent corresponds to a higher efficiency of the PEC device for hydrogen evolution. Fig. 12 shows the photocurrent density for pristine Cu_2O (A), $BaTiO_3$ (B) and $BaTiO_3/Cu_2O$ heterojunction (C,D,E,F) samples. Pristine $BaTiO_3$ thin film shows photo current density of 0.02 mA/cm^2 in comparison to $BaTiO_3/Cu_2O$ heterojunc-

Table 5
Photochemical performance of pristine Cu_2O, $BaTiO_3$ and $BaTiO_3/Cu_2O$ heterojunction Photoelectrodes.

Sample ID	Resistivity ($x10^6\ \Omega$ cm)	Photocurrent Density at 0.95 V/SCE ($mAcm^{-2}$)	ABPE Efficiency at 0.95 V/SCE
A	3.5	0.35	0.12
B	4.2	−0.02	0.006
C	2.8	0.81	0.33
D	2.1	1.44	0.66
E	2.5	0.88	0.375
F	3.2	0.60	0.22

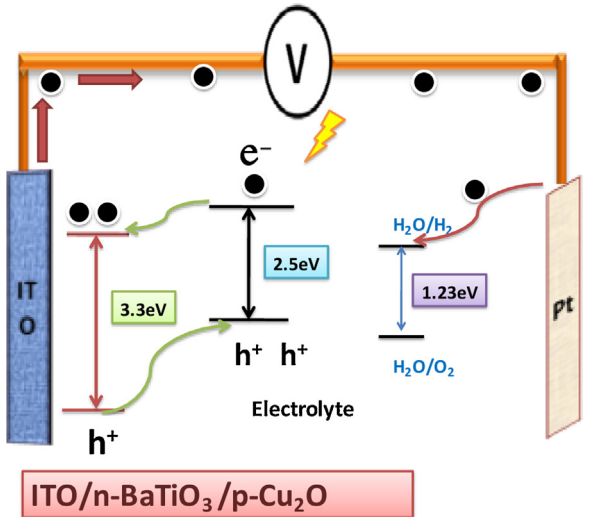

Fig. 13. Schematic energy band diagram of Cu_2O and $BaTiO_3$ heterojunction under UV–vis light illumination.

tion (sample D) of 1.44 mA/cm^2 at 0.95 V/SCE. This can be attributed to enhanced separation of photogenerated charge carriers (electrons and holes). However, the photocurrent density increases only upto 286 nm thick Cu_2O thin film after which it gradually decreases with increase in thickness of Cu_2O thin film. This may be due to excessive amount of Cu_2O that may be blocking the light absorption of $BaTiO_3$ and thereby reducing the interaction between the sample and the electrolyte leading to increase in charge recombination in the Cu_2O due to its short exciton diffusion length. [55,56]. Maximum photocurrent density obtained for $BaTiO_3/Cu_2O$ and it to be stable under illumination without any loss may be due to effective separation of photogenerated charge carriers. Other possible causes of marked increase in the photoresponse like the resistivity of the samples were calculated as presented in Table 5. Furthermore maximum value of flatband potential exhibited by sample 'D' supports maximum photocurrent density [57].

4.2.7. Charge transfer mechanism

As discussed above, the enhancement in the photocurrent density in case $BaTiO_3/Cu_2O$ heterojunction, indicate the formation of *p-n* junction between $BaTiO_3$ and Cu_2O that leads to separation of photogenerated electron-hole pairs under an internal electrostatic field gradient at the interface region of $BaTiO_3$ and Cu_2O. The excited electrons on the conduction band of the Cu_2O get transferred to $BaTiO_3$ and further to the counter electrode through external circuit. Simultaneously, holes transfer from $BaTiO_3$ to Cu_2O preventing the photocorrosion of Cu_2O [58] as shown in Fig. 6 & 13. This transfer of charge carriers is also in agreement with theoretical results described earlier. Similar type of mechanism for *p-n* junction only with experimental studies has also been

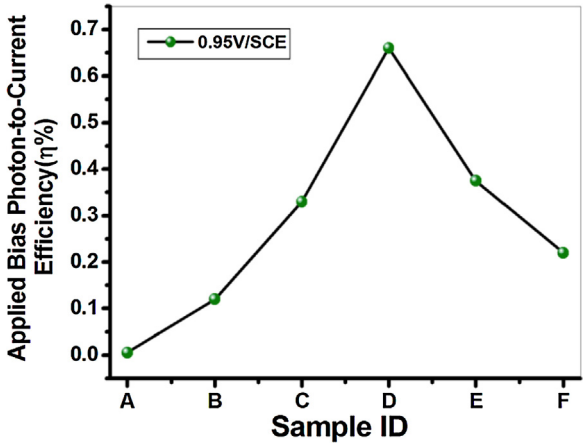

Fig. 14. Applied bias photon-to-current efficiency (ABPE) versus Sample ID curve for pristine Cu_2O (A), $BaTiO_3$ (B) and $BaTiO_3/Cu_2O$ heterojunction (C, D, E, F) thin films.

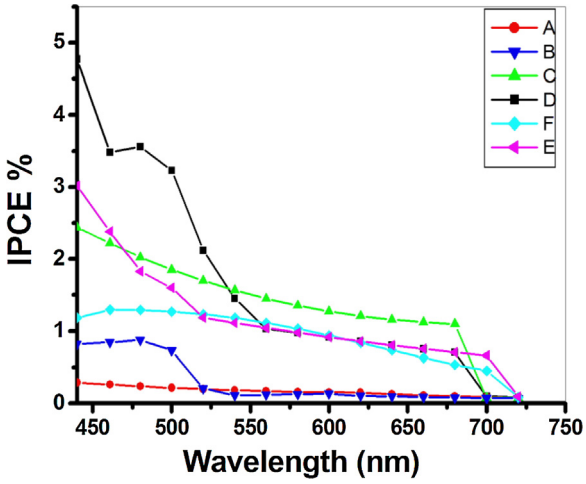

Fig. 15. IPCE performance of Pristine Cu_2O (A), $BaTiO_3$ (B) and $BaTiO_3/Cu_2O$ heterojunction samples C,D,E,F with varying upper layer thickness of Cu_2O in 0.1 M NaOH electrolytic solution.

reported earlier in case of TiO_2/Si [59], CuO/ZnO [60], $CuFe_2O_4/TiO_2$ [61], and Cu_2O/TiO_2 [62], and MoS_2/CdS heterojunction [63].

4.2.8. Efficiency calculation

The applied bias to incident photon conversion efficiency of a PEC, for the water splitting reaction can be determined by the following expression [64]:

$$\eta(\%) = [(\text{totalpoweroutput} - \text{electricalpoweroutput})/\text{lightpowerinput}] \times 100 = [J_P(E^\circ_{rev} - E_{app})/I^\circ] \times 100$$

where Jp is the photocurrent density in mA/cm^2 and E°_{rev} is the standard reversible potential for water splitting (1.23 V), $E_{app} = E_{meas} - E_{oc}$, where Emeas is the electrode potential (V/SCE) of the working electrode corresponding to the measured Jp, and E_{oc} is the open circuit potential (V/SCE) of the same working electrode under the same conditions of illumination and electrolyte. At $I^\circ = 150\ mWcm^{-2}$ efficiency was of 0.66% at 0.95 V/SCE was obtained for sample 'D' shown in Fig. 14. To quantitatively investigate the photoelectrochemical activity of the $BaTiO_3$ and $BaTiO_3/Cu_2O$ as a function of wavelength in the range of 440–730 nm, the IPCE measurements were performed for all pristine and heterojunction samples at 0.95 V/SCE and the results are presented in Fig. 15. Compared to the pristine thin film samples,

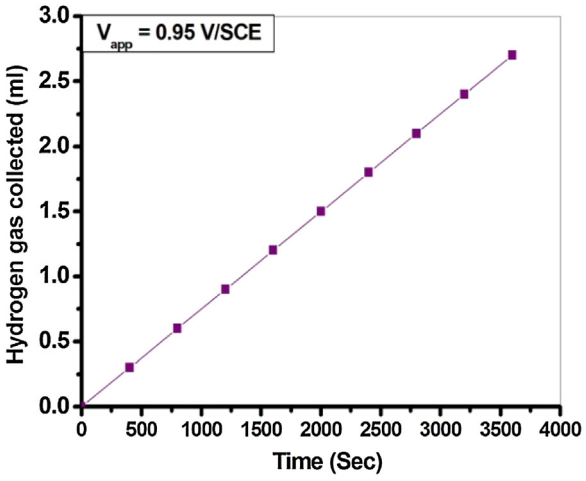

Fig. 16. Rate of hydrogen collection for the sample 'D' under light irradiance of 150 mW cm^{-2} at the position of sample.

the $BaTiO_3/Cu_2O$ films exhibit obviously enhanced IPCE values. $BaTiO_3/Cu_2O$ heterojunction (sample D) offered the highest IPCE of over 4.8% at 480 nm, which gradually decreased to zero at 700 nm. This behaviour is in line with that of the Cu_2O photoelectrode. The large increase of IPCE indicates that the heterojunction offered better harvesting of incident photons and have well aligned band edges for effective charge separation to induce PEC water splitting [65]. Similar results are also reported by Su, et al. reported IPCE 12% at 0.5 V for $WO_3/BiVO_4$ heterojunction [66]. Hydrogen generated at Pt counter electrode of PEC cell during the photoelectrochemical reaction was collected and measured by displacing water in an inverted test tube at 0.95 V/SCE (electrode potential, at which maximum ABPE was obtained) for the best photoresponsive heterojunction sample. Plot for hydrogen gas evolved with time has been shown in Fig. 16 exhibited maximum rate of production of hydrogen as 2.44 mL h^{-1} cm^{-2}. For the stability of the photoelectrode, experiment was run for multiple scans (10 times) and no change in the physical appearance of the sample was observed. Also, a linear plot obtained for amount of hydrogen generated with time evidences the stability of the photoelectrode in electrolyte for water splitting reactions.

5. Conclusions

The present study showed that $BaTiO_3$, Cu_2O *p-n* junction with varying thickness of Cu_2O thin films offers better charge separation of photogenerated charge carriers and reduction in resistance and improved light absorption ability, when used as photoelectrode in PEC cell for splitting of water to generate hydrogen using solar energy, as compared to single material photoelectrode. DFT based calculations attempted apparently for the first time in PEC studies for band off sets and effective mass for electron and holes in order to explain charge carriers separation at $BaTiO_3/Cu_2O$ interface agrees well with experiment and provides a qualitative picture of the charge separation mechanism. The maximum conversion efficiency of 0.66% was exhibited by $BaTiO_3/Cu_2O$ heterojunction photoelectrode with overall thickness 442 nm as compared to Fe-TiO_2/Zn-Fe_2O_3 heterojunction [67].

Acknowledgements

Authors gratefully acknowledge financial support received from the Department of Science & Technology, New Delhi, India, vide project no. SR/NM/NS-147/2010. Dipika Sharma is thankful to DST for providing Inspire Fellowship. We are also thankful to Dr. Saif Khan IUAC, New Delhi, India for Cross-SEM analysis of samples.

References

[1] B.O. O'Regan, M.A. Grätzel, Low-cost, high-efficiency solar cell based on dye-sensitized colloidal TiO_2 films, Nature 335 (1991) 737–740.
[2] K.H. Reddy, S. Martha, K.M. Parida, Facile fabrication of Bi_2O_3/Bi-$NaTaO_3$ photocatalysts for hydrogen generation under visible light irradiation, RSC Adv. 2 (2012) 9423–9436.
[3] Upadhyay Sumant, Shrivastava Jaya, Solanki Anjana, Choudhary Surbhi, Sharma Vidhika, Kumar Pushpendra, et al., Enhanced photoelectrochemical response of BaTiO3 with Fe doping: experiments and first-principles analysis, J. Phys. Chem. C 115 (2011) 24373–24380.
[4] K.H. Reddy, K.M. Parida, Fabrication, characterization, and photoelectrochemical properties of Cu-doped $PbTiO_3$ and its hydrogen production activity, ChemCatChem 5 (2013) 3812–3820.
[5] Solanki Anjana, Shrivastava Jaya, Upadhyay Sumant, Sharma Vidhika, Sharma Poonam, Kumar Pushpendra, et al., Irradiation-induced modifications and PEC response: a case study of SrTiO3 thin films irradiated by 120 MeV Ag^{9+} ions, Int. J. Hydrogen Energy 3 (2011) 5236–5245.
[6] A. Nashim, S. Martha, K.M. Parida, Gd2Ti2O7/In2O3: an efficient visible light driven heterojunction based composite photocatalysts for hydrogen production, ChemCatChem 5 (2013) 2352–2359.
[7] Choudhary Surbhi, Upadhyay Sumant, Kumar Pushpendra, Singh Nirupama, Satsangi R. Vibha, Shrivastav Rohit, Nanostructured bilayered thin films in photoelectrochemical water splitting: a review, Int. J. Hydrogen Energy 37 (2012) 18713–18730.
[8] P.D. Tran, L.H. Wong, J. Barber, J.S.C. Loo, Recent advances in hybrid photocatalysts 337 for solar fuel production, Energy Environ. Sci. 5 (2012) 5902–5918.
[9] Y. Li, J.Z. Zhang, Hydrogen generation from photoelectrochemical water splitting based on nanomaterials, Laser Photonics Rev. 4 (2010) 517–528.
[10] R. Van de Krol, Y. Liang, J. Schoonman, Solar hydrogen production with nanostructured metal oxides, J. Mater. Chem. 18 (2008) 2311–2320.
[11] M.R. Allen, A. Thibert, E.M. Sabio, N.D. Browning, D.S. Larsen, F.E. Osterloh, Evolution of physical and photocatalytic properties in the layered titanates A2Ti4O9 (A = K, H) and in nanosheets derived by chemical exfoliation, Chem. Mater. 22 (2010) 1220–1228.
[12] W. Yao, C. Huang, J. Ye, Hydrogen production and characterization 346 of LaSrNb2NiO9 (M = Na, Cs, H) based photocatalysts, Chem. Mater. 22 (2010) 1107–1113.
[13] K. Maeda, T.E. Mallouk, Comparison of two- and three-layer restacked Dion—Jacobson 350 phase niobate nanosheets as catalysts for photochemical hydrogen evolution, J. Mater. Chem. 19 (2009) 4813–4818.
[14] R. Ma, Y. Kobayashi, W.J. Youngblood, T.E. Mallouk, Potassium niobate nanoscrolls incorporating rhodium hydroxide nanoparticles for photocatalytichydrogen evolution, J. Mater. Chem. 18 (2008) 5982–5985.
[15] K. Maeda, M. Eguchi, W.J. Youngblood, T.E. Mallouk, Calcium niobate nanosheets prepared by the polymerized complex method as catalytic materials for photochemical hydrogen evolution, Chem. Mater. 21 (2009) 3611–3617.
[16] Y. Miseki, H. Kato, A. Kudo, Water splitting into H2 and O2 over niobate and titanate photocatalysts with (111) plane-type layered perovskite structure, Energy Environ. Sci. 2 (2009) 306–314.
[17] H.G. Kim, D.W. Hwang, J. Kim, Y.G. Kim, J.S. Lee, Highly donor-doped (110) layered perovskite materials as novel photocatalysts for overall water splitting, Chem. Commun. 12 (1999) 1077–1078.
[18] T. Takata, Y. Furumi, K. Shinohara, A. Tanaka, M. Hara, J.N. Kondo, K. Domen, Photocatalytic decomposition of water on spontaneously hydrated layered perovskites, Chem. Mater. 9 (1997) 1063–1064.
[19] D.W. Hwang, H.G. Kim, J. Kim, K.Y. Cha, Y.G. Kim, J.S. Lee, Photocatalytic water splitting over highly donor-doped (110) layered perovskites, J. Catal. 193 (369) (2000) 40–48.
[20] K. Saito, A. Kudo, Niobium-complex-based syntheses of sodium niobate nanowires possessing superior photocatalytic properties, Inorg. Chem. 49 (2010) 2017–2019.
[21] D. Kan, T. Terashima, Y. Shimakawa, M. Takano, Fabrication and I-V characteristics of p-n junctions composed of high-Tc superconductors and La-doped SrTiO3, Thin Solid Films 486 (2005) 71–74.
[22] Q.W. Tang, L. Lin, Z.P. Mao, J.H. Wu, P-N heterojunction on dye-sensitized ZnO nanorod arrays and macroporous polyaniline network, RSC Adv. 2 (2012) 1863–1869 (23).
[23] X.F. Liu, Y.L. Li, One-dimensional hybrid nanostructures with light-controlled properties, Dalton Trans. 33 (2009) 6447–6457.
[24] Y. Huang, X.F. Duan, C.M. Lieber, Nanowires for integrated multicolor nanophotonics, Small 1 (2005) 142–147.
[25] Y.J. Zhang, H.L. Dong, Q.X. Tang, S. Ferdous, F. Liu, S.C.B. Mannsfeld, W.P. Hu, A.L. Briseno, Organic single-crystalline p-n junction nanoribbons, J. Am. Chem. Soc. 132 (2010) 11580–11584.
[26] J. Wang, W.D. Zhang, Fabrication of CuO nanoplatelets for highly sensitive enzyme-free determination of glucose, Electrochim. Acta 56 (2011) 7510–7516.
[27] M. Kohno, T. Kaneko, S. Ogura, K. Sato, Y. Inoue, Dispersion of ruthenium oxide on barium titanates (Ba6Ti17O40, Ba4Ti13O30, BaTi4O9 and

Ba2Ti9O20) and photocatalytic activity for water decomposition, Chem. Soc. Faraday Trans. 94 (1998) 89–94.
[28] Y. Yu, F.P. Du, J.C. Yu, P.K. Wong, One dimensional shapecontrolled preparation of porous Cu_2O nano-whiskers by using CTAB as a template, J. Solid State Chem. 177 (2004) 4640–4647.
[29] Solanki Anjana, Shrivastava Jaya, Upadhyay Sumant, Choudhary Surabhi, et al., Modified structural, morphological and photoelectrochemical properties of 120 MeV Ag^{9+} ion irradiated BaTiO3 thin films, Curr. Appl. Phys. 13 (2013) 344–350.
[30] Kosugi Tsuyoshi, Kaneko Shoji, Novel spray-pyrolysis deposition of cuprous oxide thin films, J. Am. Ceram. Soc. 81 (1998) 3117–3124.
[31] N.T. Hahn, H. Ye, D.W. Flaherty, A.J. Bard, C.B. Mullins, Reactive ballistic deposition of $-Fe_2O_3$ thin films for photoelectrochemical water oxidation, ACS Nano 4 (2010) 1977–1986.
[32] Sandro Scandolo, Paolo Giannozzi, Carlo Cavazzoni, Stefano de Gironcoli, Pasquarello Alfredo and Baronil Stefano, Z., Kristallogr, QUANTUM ESPRESSO: a modular and open-source software project for the quantum simulation of materials, 2005, 220, 574-582582582582.
[33] J.P. Perdew, K. Burke, M. Ernzerh, Generalized gradient approximation made simple, Phys. Rev. Lett. 77 (1996) 3865–3872.
[34] D. Vanderbilt, Soft self-consistent pseudopotentials in a generalized eigenvalue formalism, Phys. Rev. B 41 (1990) 7892–7899.
[35] H.J. Monkhorst, J.D. Pack, On special points for brillouin zone integrations, Phys. Rev. B 13 (1976) 5188–5193.
[36] L. Colombo, R. Resta, S. Baroni, Valence-band offsets at strained Si/Ge interfaces, Phys. Rev. B 44 (1991) 5572.
[37] M. Peressi, N. Binggeli, A. Baldereschi, Band engineering at interfaces: theory and numerical experiments, Phys. D: Appl. Phys. 35 (1998) 1273.
[38] C.G. Van de Walle, R.M. Martin, Theoretical study of band offsets at semiconductor interfaces, Phys. Rev. B 35 (1987) 8154.
[39] Hongliang Shi, Hui Pan, Yong-Wei Zhang, Boris I. Yakobson, Quasiparticle band structures and optical properties of strained monolayer MoS2 and WS2, Cond. Matter Mater. Sci. (2013) 1–8.
[40] M. French, R. Schwartz, H. Stolz, R. Redmer, Electronic band structure of Cu_2O by spin density functional theory, J. Phys. Condens. Matter 21 (2009) 1.
[41] Sonali Saha, T.P. Sinha, Electronic structure, chemical bonding and optical properties of paraelectric $BaTiO_3$, Phys. Rev. B (2000) 62.
[42] Y. Ching, Yong Xu Nian, W.K. Wong, Ground-state and optical properties of Cu_2O and CuO crystals, Phys. Rev. B 40 (1989) 7684.
[43] Keigo Suzuki, Kazunori Kijima, Optical band gap of barium titanate nanoparticles prepared by RF-plasma chemical vapor deposition, Japanese, J. App. Phys. 44 (2005) 2081–2082.
[44] J. Hensel, G. Wang, Y. Li, J.Z. Zhang, Synergistic effect of CdSe Quantum dot sensitization and nitrogen doping of TiO2 nanostructures for photoelectrochemical solar hydrogen generation, Nano Lett. 10 (2010) 478–483.
[45] Jingling Liu, Muhammad Ko Shahid, Seon Young, Eunchul Kim, Tae Kyu Ahn, Jong Hyeok, et al., Investigation of porosity and heterojunction effects of a mesoporous hematite electrode on photoelectrochemical water splitting, Phys. Chem. Chem. Phys. 15 (2013) 9775–9782.
[47] Yanchao Mao, Jintian He, Xiaofeng Sun, Wei Li, Xihong Lu, Jiayong Gana, et al., Electrochemical synthesis of hierarchical Cu_2O stars with enhanced photoelectrochemical properties, Electrochim. Acta 62 (2012) 1–7.
[48] R.D. Shannon, Crystal physics, diffraction, theoretical and general crystallography, Acta Cryst. A 32 (1976) 751–767.
[49] Lei Huanga, Feng Peng, S. Ohuchi Fumio, In situ XPS study of band structures at Cu_2O/TiO_2 heterojunctions interface, Surf. Sci. 603 (2009) 2825–2832.
[50] S. Poulston, P.M. Parlett, P. Stone And, M. Bowker, Surface oxidation and reduction of Cuo And Cu_2o studied using xps and xaes, Surf. Interface Anal. 24 (1996) 811–820.
[51] Batakrushna Santara, P.K. Giri, Kenji Imakita, Minoru Fujii, Evidence for Ti interstitial induced extended visible absorption and near infrared photoluminescence from undoped TiO_2 anoribbons: an in situ photoluminescence study, J. Phys. Chem. C 117 (2013) 23402–23411.
[52] T.C. Dang, D.L. Pham, H.C. Le, V.H. Pham, TiO_2/CdS nanocomposite films: fabrication, characterization,electronic and optical properties, Adv. Nat. Sci. Nanosci. Nanotechnol. 1 (2010) 2043–6254.
[53] J.W. Schultze, U. Stimming, J. Weise, Capacity and photocurrent measurements at passive titanium electrodes, Ber Bunsenges Phys. Chem. 86 (1982) 276–282.
[54] Aadesh P. Singh, Saroj Kumari, Rohit Shrivastav, Sahab Dass, Vibha R. Satsangi, Improved photoelectrochemical response of haematite by high energy Ag^{+9} ions irradiation, J. Phys. D Appl. Phys. 42 (2009) 08530–08538.
[55] Aiming Mao, Kyu Kim Jung, Kahee Shin, Hwan Wang Dong, Pil Yoo, Hematite modified tungsten trioxide nanoparticle photoanode for solar water oxidation, J. Power Sour. 210 (2012) 32–37.
[56] Junying Zhang, Hailing Zhu, Shukai Zheng, Feng Pan, Wang Tianmin TiO_2/Cu_2O microgrid heterojunction with photocatalytic activity under solar light irradiation, Appl. Mater. Interfaces 1 (2009) 2111–2114.
[57] Poonam Sharma, Praveen Kumar, Anjana Solanki, Rohit Shrivastav, Sahab Dass, Vibha R. Satsangi, Satsangi nanostructured Zn-Fe_2O_3 thin film modified by Fe-TiO_2 for photoelectrochemical generation of hydrogen, Int. J. Hydrogen Energy 35 (2010) 10883–10889.
[58] Dipika Sharma, Anuradha Verma, V.R. Satsangi, Rohit shrivastav, Sahab Dass, Nanostructured $SrTiO_3$ thin films sensitized by Cu_2O for photoelectrochemical hydrogen, Int. J. Hydrogen Energy 39 (2014) 4289–4299.
[59] Sun Young Noh, et al., Branched TiO_2/Si nanostructures for enhanced photoelectrochemical water splitting, Nano Energy 2 (2013) 351–360.
[60] K.K. Baek, H.L. Tuller, Atmosphere sensitive CuO/ZnO junctions, Solid State Ionics 75 (1995) 179–191.
[61] A. Kezzim, N. Nasrallah, A. Abdi, M. Trari, Visible light induced hydrogen on the novel hetero-system $CuFe_2O_4/TiO_2$, Energy Convers. Manag. 52 (2011) 2785–3074.
[62] W. Siripala, A. Ivanovskaya, T.F. Jaramillo, S.H. Beck, E.W. Mcfarland, A Cu_2O/TiO_2 heterojunction thin Film cathode for photoelectrocatalysis, Sol. Energy Mater. Sol. Cells 77 (2003) 229–237.
[63] Ying Liu, Yu-Xiang Yu, Wei-De Zhang, MoS_2/CdS heterojunction with high photoelectrochemical activity for H_2 evolution under visible light: the role of MoS_2, J. Phys. Chem. C 117 (2013) 12949–12957.
[64] W.B. Ingler, S.U.M. Khan, Photoresponse of spray pyrolytically synthesized magnesium-doped iron(III) oxide (p-Fe2O3) thin films under solar simulated light illumination, Thin Solid Films 461 (2004) 301–308.
[65] C.-F. Chi, Y.-L. Lee, H.-S. Weng, A CdS-modified TiO_2 nanocrystalline photoanode for efficient hydrogen generation by visible light, Nanotechnology 19 (2008) 125704–125709.
[66] Jinzhan Su, Liejin Guo, Ningzhong Bao, Grimes A. Craig, Nanostructured $WO_3/BiVO_4$ heterojunction films for efficient photoelectrochemical water splitting, Nano Lett. 11 (2011) 1928–1933.
[67] Poonam Sharma, Praveen Kumar, Anjana Solanki, Rohit Shrivastav, Sahab Dass, Vibha R. Satsangi, Photoelectrochemical performance of bilayered Fe–TiO_2/Zn–Fe_2O_3 thin films for solar generation of hydrogen, J. Solid State Electrochem. 16 (2012) 1305–1312.